

## Rice monitoring and production estimation using multitemporal RADARSAT

Yun Shao<sup>a,\*</sup>, Xiangtao Fan<sup>a,b</sup>, Hao Liu<sup>a</sup>, Jianhua Xiao<sup>a</sup>, S. Ross<sup>c</sup>, B. Brisco<sup>d</sup>,  
R. Brown<sup>c</sup>, G. Staples<sup>e</sup>

<sup>a</sup>Laboratory of Remote Sensing Information Sciences, Institute of Remote Sensing Applications, Chinese Academy of Sciences, Beijing 100101, People's Republic of China

<sup>b</sup>Department of Earth Sciences, Nanjing University, Nanjing, People's Republic of China

<sup>c</sup>Canada Center for Remote Sensing, Ottawa, Ontario, Canada

<sup>d</sup>Noetix Research, Ottawa, Ontario, Canada

<sup>e</sup>RADARSAT International, Vancouver, British Columbia, Canada

Received 22 March 2000; accepted 18 November 2000

### Abstract

Rice monitoring and production estimation has special significance to China, as rice is the staple grain and accounts for 42% of the crop production in this country. Radar remote sensing is appropriate for monitoring rice because the areas where this crop is cultivated are often cloudy and rainy. Synthetic Aperture Radar (SAR) is thus anticipated to be the dominant high-resolution remote sensing data source for agricultural applications in tropical and subtropical regions. It also provides revisit schedules suitable for agricultural monitoring. This paper presents the results of a study examining the backscatter behavior of rice as a function of time using multitemporal RADARSAT data acquired in 1996 and 1997. A rice-type distribution map was produced, showing four types of rice with different life spans ranging from 80 days to 120–125 days. The life span of a rice crop has significant impact on the yield, as well as on the taste and quality of the rice, with the longer growing varieties having the best taste and the highest productivity. The rice production of three counties and two administrative regions, totaling 5000 km<sup>2</sup>, was estimated in this study. The accuracy of the rice classification was found to be 91% (97% after postclassification filtering) providing confidence that multitemporal RADARSAT data is capable of rice mapping. An empirical growth model was then applied to the results of the rice classification, which related radar backscatter values to rice life spans. These life spans could then be used to sum up the production estimates, which were obtained from agronomic models already in use for rice by local agronomists. These models related the yield of rice to their life span based on empirical observations for each type of rice. The resulting productivity estimate could not be compared to any other existing data on yield production for the study-area, but was well received by the local authorities. Based on the studies carried out in the Zhaoqing test site since 1993, it is suggested that rice production estimates require three radar data acquisitions taken at three different stages of crop growth and development. These three growth stages are: at the end of the transplanting and seedling development period, during the ear differentiation period, and at the beginning of the harvest period. Alternatively, if multiparameter radar data is available, only two data acquisitions may be needed. These would be at the end of the transplanting and seedling development period, and at the beginning of the harvest period. This paper also proposes an operational scenario for rice monitoring and production estimation. © 2001 Elsevier Science Inc. All rights reserved.

### 1. Introduction

Rice is a heat and water-loving crop. Most paddy rice in the world grows in warm, humid environments with heavy cloud cover and rainfall. Thus, it is difficult to acquire

optical remote sensing data in rice growing regions. Synthetic Aperture Radar (SAR), with “all-weather,” day or night imaging capabilities and frequent revisits, is anticipated to be the dominant high-resolution remote sensing data source for agriculture monitoring in tropical and subtropical regions. SAR data not only provides data when optical remote sensing data is impossible to acquire, but also provides information about the geometric structure and moisture content of the vegetation, which is needed by agronomists and other end-users. Rice monitor-

\* Corresponding author. Tel.: +86-10-648-76313; fax: +86-10-648-76313.

E-mail address: yunshao@public.bta.net.cn (Y. Shao).

ing and production estimation have special significance to China, as rice is the staple grain and accounts for 42% of the crop production in this country. The estimation of crop yield and production is a topic of global interest (McDonald & Hall, 1980), and the efficient management of agricultural land resources is strongly related to social and economically sustainable development, especially important in China.

It is well known that China has the largest population of any country. As the population increases, and the economy and industry develop, the quantity and quality of cultivated land are decreasing rapidly. The food supply for the current 1.2 billion people is a serious concern facing China, and will intensify as the population continues to grow. Therefore, it is important to find an efficient way to face this dilemma. Crop production information is also important for China in order for the authorities to manage and adjust the grain distribution within the nation. Remote sensing technology can provide timely and accurate information about crop distribution, area planted, and potential production for decision makers at many levels. In fact, since national reform started 20 years ago, the structure of farming activities has changed dramatically because farmers have turned from a planning economy to a market economy. With this shift, decisions with respect to farming activities are left up to the farmer. Information on crop production estimation is therefore significant to government agencies, as well as to the farmers, and may help in planning farming activities and marketing strategies early in the season.

The use of microwave remote sensing technology to study ecological systems is becoming more and more popular among the world's scientific community (Dobson, Pierce, Sarabandi, Ulaby, & Sharik, 1992; Kasischke & Christensen, 1990). Scientists have carried out extensive field measurement campaigns (Ulaby, Moore, & Fung, 1981–1986), airborne flight missions (Campbell, Ryerson, & Brown, 1995; Guo, Wang, Liao, Shao, & Wei, 1995; Shao, Guo, Liu, Li, & Lu, 1995a; Shao et al., 1995b; Zebker et al., 1991; Guo et al., 1997), and spaceborne missions (Stofan et al., 1995), in order to better understand the earth biosphere. Many microwave backscatter models were developed to study the backscatter behavior of vegetation (Chauhan, LeVine, & Lang, 1994; Karam & Fung, 1988; Matzler, 1994; Ulaby, Sarabandi, McDonald, Whitt, & Dobson, 1990; El-Reyes & Ulaba, 1987). Although there is more literature available on research for forest applications than for agricultural applications (Brisco & Brown 1998; Engheta & Elachi, 1982; Freeman, Durden, & Zimmerman, 1992; Ulaby et al., 1990), there are still many successful examples in radar remote sensing for agricultural applications (Anys & He, 1995; Le Toan, Laur, Mougin, & Lopes, 1989; Schotten, van Rooy, & Jansen, 1995; Shao, Guo, Liu, & Lu, 1996; Soares, Bernard, & Vidal-Madjar, 1987; Soares, Renn, Formaggio, Yanasse, & Frery, 1997; Ulaby, Li, & Shanmugan, 1982). However, only a few papers specifically focus on rice monitoring (Kurosu, Fujita, &

Chiba, 1995, 1997; Le Toan et al., 1997; Liu, Shao, & Wang, 1997; Shao, Fan, Wang, & Liu, 1997; Shao, Liu, Lu, & Guo, 1997; Shao, Verjee, & Staples, 1997; Shao, Wang, Fang, & Liu, 1997). The results reported on rice monitoring using SAR technology were very promising, encouraging us to look at the potential of RADARSAT data for rice area calculation and estimation of the life span of the rice, which are essential pieces of information in order to produce a production forecast.

This paper presents the results of a study examining the backscatter behavior of rice as a function of time using multitemporal RADARSAT data. A rice-type distribution map was produced, showing four types of rice with different life spans ranging from 80 to 120–125 days. The life span of a rice crop has a significant impact on the yield, as well as on the taste and quality of the rice. The rice production for three counties and two administrative regions, totaling 5000 km<sup>2</sup>, was then estimated using multitemporal RADARSAT data. Using results obtained from analyses of multiparameter data sets acquired by Shuttle Imaging Radar C-band (SIR-C)/X-band SAR (X-SAR) in 1994 and the Canada Centre for Remote Sensing (CCRS) CV-580 in 1993, the backscatter behavior of rice as a function of frequency is also discussed. This paper concludes with an operational scenario for rice monitoring and production estimation.

The objectives of this study were:

1. to understand the backscatter behavior of rice over its entire growth cycle;
2. to precisely delineate the distribution and calculate the area of rice cultivation;
3. to identify rice crops with different life spans, which has a key impact on production and quality;
4. to evaluate the capability of RADARSAT data for rice crop identification and its potential contribution to rice production estimation; and
5. to propose an operational scenario for using RADARSAT data in rice crop monitoring and production estimation in the future.

## 2. Background

### 2.1. Rice distribution in China

Rice plantations are widely distributed throughout China. Based on statistics from 1991 (Zhao ed., 1996), rice plantations in China covered an area of 330,640 km<sup>2</sup>, and accounted for 22.7% of the rice plantations in the world. The total yield of rice in China was 19.1 million tons, which was 37% of the world's total rice production. The yield per hectare was 5.799 tons, which is 1.63 times the world's average rice yield. Although the cultivated area of rice in China is only about 30% of the total agricultural land, the production of rice accounts for 42% of the total crop

production of the country. As the demand for rice increases as a function of an increasing global population, it is estimated that global rice production will need to double by the year 2020.

The majority (90%) of rice cultivation in China is distributed throughout southern and east central China, mainly in the downstream portions of the Yangtze River, specifically in Guangdong, Guangxi, Yunnan, and Guizhou Provinces, and the southern part of Shanxi and Henan Provinces. In this region, there is a plentiful supply of water and warm temperatures to allow for rice to develop easily and quickly. However, there are less than 50 clear days per year in the area south of the Yangtze River, where the majority of the rice grows. With mostly rainy and cloudy weather, optical remote sensing for rice monitoring is limited. Radar's "all-weather" capabilities make it a useful tool in this type of environment.

### 2.2. Ecology of rice (Zhao et al., 1996)

Rice grows in specific ecological conditions and geographic regions. The following factors have a critical influence on rice distribution and yield.

(1) Temperature is the most influential factor determining the distribution of rice plantations. Typically, if the region has an annual accumulated temperature (in degree-days) of 2000–4500°C for  $\geq 10^\circ\text{C}$ , there is only one rice crop a year. If the annual accumulated temperature is 4500–7000°C for  $\geq 10^\circ\text{C}$ , there can be two rice crops a year with an accumulated temperature of 5300°C for  $\geq 10^\circ\text{C}$  being the safe point for two rice crops a year. Three rice crops a year can be produced with an annual accumulated temperature of 7000°C for  $\geq 10^\circ\text{C}$ .

(2) Water supply and availability is another important factor in determining the distribution of rice production. The water-supply to a particular rice field is largely determined by rainfall, irrigation, evaporation, and soil-permeability.

(3) Solar illumination duration determines the rice species, its distribution, and yield. Some species need more sun than others.

(4) Elevation is related to temperature, and rice can only be grown below a certain elevation. This varies with latitude and local temperature.

(5) Rice plants prefer soil with good water-holding capacity, fertility, permeability, and a middle pH value. Sandy or clay soil is usually most suitable.

According to natural environmental conditions, especially meteorological conditions and the biological index of rice, a rice yield estimation model can be established for any given region. There are a number of rice yield estimation models which can be used to estimate rice yield (Zhao et al., 1996), most of which rely on meteorological data. However, these meteorologically based yield models are restricted locally as they are based on empirical observations. These empirically established yield models were available for the study site.

### 2.3. Rice species and life span

Rice species are very numerous in China, with a number of different types distributed over many geographic regions. The variety of rice species is related to annual yield, and must be taken into consideration when calculating the rice production for any given area. In China, the rice species vary with the geographic location and growing season, and thus the various life spans of the different rice varieties is an important consideration during the decision making for each farmer. According to the growing season and life span, rice can be defined as a single early crop (spring), middle rice (one crop a year), single late rice (autumn), double-cropped rice (spring and autumn), and triple rice (three crops a year). The growth seasons and crop calendars for each type are quite different. In terms of rice crop life spans, there are early mature rice, medium mature rice, medium–late mature rice, and late mature rice. In the Zhaoqing test site, the life span of early mature rice is 80 days, and the yield is about 300–350 kg/mu.<sup>1</sup> The life span of medium mature rice is 110–115 days, producing a yield of about 400–450 kg/mu. Medium–late mature rice has a life span of 115–120 days, and a yield of about 450–500 kg/mu. For late mature rice, the life span is 125 days, and the yield is 500–550 kg/mu. In general, the longer the life span of rice, the higher the yield will be. It is therefore essential to collect the statistics of rice acreage in accordance with the rice species, life span, and growing season. In addition, the geographic location, water supply, temperature, fertilizer, and tillage practices will affect the crop yield. Although trends are often present in yield estimations, the exact yield usually varies from one field to another. It is important to note once again that rice yield estimation models can only be applied to a specific geographic region, and may need to be modified according to local conditions.

### 2.4. Rice growth calendar

In the Zhaoqing test site, there are two crops per year: early season (spring) rice and late season (autumn) rice. There are five major growth periods in the life cycle of rice. (1) Transplanting period: rice plant seedlings are transplanted from the seedbed to the paddy field with the transplanting date depending on the weather, especially temperature. (2) Seedling development period: the seedling begins to develop a root system and starts tillering during the vegetative growth stage. (3) Ear differentiation period: end of vegetative growth to start of reproductive stage. (4) Heading period: rice heads begin to form during the reproductive stage. (5) Maturation period: the rice plants mature and are ready to be harvested. Temporally, these five periods for early season rice are March 25–April 5, April 15–25, May 10–30, June 10–25, July 5–31. For late

<sup>1</sup> Mu is a Chinese area measurement unit, 1 mu equals 666.66 m<sup>2</sup>.

season rice, the growth stages occur as follows: July 20–August 5, August 10–20, September 1–30, October 1–20, November 1–25. The exact dates of each period vary with the weather conditions during the entire life cycle of the rice. Plant maturity rates and life spans are species-dependent. This rice calendar described above illustrates a typical rice growth behavior in the Zhaoqing test site. It will vary with the geographic location, ecological conditions, and local climate.

With progress in agricultural technology, it is known that a long growing season is favorable to high photosynthetic rates and subsequently high rice yields. For this reason, the transplanting date of rice is getting earlier, and the life span is getting longer. For example, the local farmers grew three rice crops a year in the past, but now they only grow two crops a year. In the USA, there is only one rice crop a year. It starts in early May with harvest near the end of October. This rice life cycle is around 170–180 days with yields reaching 6.2 tons/ha, which is higher than the rice yield in China (5.8 tons/ha). Improved varieties and cultural practices have contributed significantly to increased rice yields in the last few decades as well.

### 3. Test site and data description

This study was carried out in the Zhaoqing test site located in Guangdong Province in southern China, centered at latitude 22.30N, longitude 112.30E. This site is located at the northwestern end of the Pearl River Delta. Zhaoqing is the only rice-producing region in the Pearl River Delta with a surplus of rice production, which means that the area produces a self-supply of grain, as well as provides grain for export to other areas in the Pearl River Delta region. The

Pearl River Delta is the fastest growing economical area in China, with a high population density. Relative to the population density, cultivated land resources are limited. In the past two decades, a great deal of land has been used for infrastructure, industry, and urban development, or the rice fields have been changed to produce more marketable crops, such as *Euryale ferox*, banana, orange, and fish farming. These farm products bring more cash, which is increasingly important in the free-market economy. The farmland of Zhaoqing is mainly located within the flood plain from 0 to 50 m. Most rice fields are located in the flood plain, with only a small number of rice fields found at higher elevations. The mountainous areas surrounding the flood plain are generally covered by forest and orchards, with little exposed rock. There are some artificial forest plantations, but mostly natural forest covers this region. The field sizes in this area are relatively small, ranging from 100 to 500 m, and are separated by narrow dirt ditches. Some of the ditches are lined with trees or high grass cover, which can give a strong return to the SAR antenna. During the early stage of rice growth, these linear features can have a significant influence on image classification, and should be taken into consideration when calculating the acreage of the rice production area.

The CCRS airborne CV-580 X/C-SAR system first imaged the test site in 1993 during the GlobeSAR mission (Shao et al., 1995b, 1996; Guo & Shao, 1997). The SIR-C and X-SAR also imaged the area on April 18, 1994 (Stofan et al., 1995). Other data sets included in this study are multitemporal RADARSAT images, which includes 13 scenes acquired from March to December in 1996 and seven scenes from April to July in 1997. The system parameters, imaging modes, and acquisition dates of the SAR data used in this study are listed in Table 1. For the Zhaoqing test site,

Table 1  
System parameters of SAR data

| Data source            |                      |       |                      |     |     |  |  |
|------------------------|----------------------|-------|----------------------|-----|-----|--|--|
| Parameters             | GlobeSAR             |       | SIR-C/X-SAR          |     |     | RADARSAT (fine)  | RADARSAT (standard)  |
| Frequency (GHz)        | C                    | X     | L                    | C   | X   | C  | C  |
|                        | 5.3                  | 9.25  | 1.24                 | 5.3 | 9.6 | 5.3  | 5.3  |
| Polarization           | HH,                  | HV HH | HH                   | HH  |     | HH   | HH   |
|                        | VV,                  | VH VV | HV                   | HV  |     |  |  |
| Incidence angle (°)    | 14–45                |       | 34.1                 |     |     | 43–46 (F4)   | 36–42 (S5), 41–46 (S6)   |
| Nominal resolution (m) | 6 × 6                |       | 25 × 25, 12.5 × 12.5 |     |     | 10 × 10  | 30 × 30  |
| Pixel spacing (m)      | 6 × 6                |       | 25 × 25              |     |     | 6.25 × 6.25  | 12.5 × 12.5  |
| Swath width (km)       | 18                   |       | 37.8                 |     |     | 50   | 100  |
| Imaging date           | Nov. 20 and 21, 1993 |       | April 18, 1994       |     |     | In 1996:<br>June 17, Aug. 4,<br>Sept. 21, Oct. 15,<br>Nov. 8, Dec. 2 | In 1996:<br>Mar. 26, Apr. 25, June 10,<br>Aug. 23, Aug. 28, Sept. 16,<br>Nov. 27<br>In 1997:<br>Apr. 25, May 19, June 4,<br>June 12, June 28, July 6,<br>July 22<br>In 1999:<br>Apr. 17, Apr. 22<br>May 11, May 16 |

Table 2  
The dates of the ground measurements for 1996 and 1997

| Season         | Measurement date  |
|----------------|---|
| Spring of 1996 | May 27, June 12, June 20, July 6, July 13                         |
| Autumn of 1996 | Aug. 23, Sept. 1, 16, and 24, Oct. 10 and 24, Nov. 4 and 8        |
| Spring of 1997 | Mar. 28, Apr. 11 and 22, May 4 and 19, June 5, 12, and 29, July 7 |

there was a 3-year continuous RADARSAT data acquisition program for rice monitoring. The first 2 years of research focused on studying the backscatter behavior of rice and the potential of RADARSAT for rice production estimation. The third year’s focus was for operational rice monitoring and production estimation (Table 1).

4. Ground observations of rice

The RADARSAT spacecraft flew over the Zhaoqing test site 6 min before 6:00 am for descending passes and 6 min after 6:00 pm for ascending passes (local time). The ground measurements of the dynamic rice parameters were taken the same day as the RADARSAT data acquisition, and other parameters were measured 1 or 2 days before or after the data acquisition. Measurements were taken for 20 rice samples from within a sample plot measuring 100 × 100 m. Recorded measurements included: measurement date, sample code, row spacing, the number of rice seedlings per cluster, height and width of the rice stem, water content of each rice cluster, and the number of leaves of a single rice plant. The leaves were numbered from bottom to top as leaves 1, 2, 3, 4, and 5 with the length, width, and the inclination angle of each leaf to the rice stem measured. Table 2 shows the dates that the ground measurements were taken. In addition, meteorological data were collected, including temperature, air pressure, relative humidity, wind speed, and direction.

5. Methodology

5.1. Backscatter studies

In order to examine the backscatter behavior of rice as a function of time and growth stage, we extracted the backscatter coefficients of different types of rice from calibrated RADARSAT images acquired in 1996 and 1997. The images acquired on August 4, September 21, October 15, November 8, and December 2 of 1996 are analyzed as one data set. The images acquired on April 25, May 19, June 4, June 12, June 29, July 6, and July 22 of 1997 are analyzed as a second data set. The calibration accuracy of the RADARSAT Fine and Standard mode products is approximately 1 dB. Both of the data sets were co-registered for this study.

First, the image digital numbers were converted to backscatter coefficients (dB) to facilitate making absolute comparisons of the backscatter behavior of rice as a function of time. Fine mode and Standard mode RADARSAT image data received by a ground station are in 16-bit unsigned integer format. The header file contains spacecraft orbit parameters and gain control factors. With spacecraft orbit parameters, we calculate the local incidence angle of each pixel across the range direction. We then use the following calibration equation for RADARSAT to convert the DN of the image to backscatter coefficients (dB) (Eq. (1)):

$$\sigma_{jk}^0 = 101g(DN_{jk}^2 + A_0)/A_j + 101g(\sin(I_j)) \tag{1}$$

DN is the digital number of RADARSAT image,  $A_0$ ,  $A_j$  is the automatic gain control factor, and  $I_j$  is the local incidence angle of each pixel across the range direction.

A sample area of 20 pixels by 20 lines is extracted from each data set to estimate the backscatter coefficient value. The probability distribution function of the 400 pixels is then inspected with the value having the highest probability among the 400 pixels chosen to represent the backscatter coefficient on the image acquisition date. In fact, a distributed target, such as rice, imaged by a SAR does not have uniform backscatter coefficients in the resulting SAR image. The values vary over a wide range because of the speckle noise inherent to SAR data, and may range from 10 to -40 dB. The histogram of a distributed target, such as rice, thus has a very diverse distribution. The same speckle noise makes a SAR image look very rough, unlike an optical remote sensing image, which is very smooth. This effect is minimized by taking a sample with enough pixels to obtain and use a representative value for the backscatter behavior of the target. We took several sample areas, examined the mean, standard deviation, the minimum value, the maximum value, and the backscatter coefficient, to ensure the backscatter coefficient value we calculated was representative. Finally, the backscatter coefficient of rice as a function of time can be plotted for each rice or land-cover type.

Based on the backscatter behavior of medium-late mature rice, an experimental backscatter model was established. It is the cubic polynomial that best simulated the backscatter coefficients of rice as a function of time as shown in Fig. 1. This model was based on the knowledge

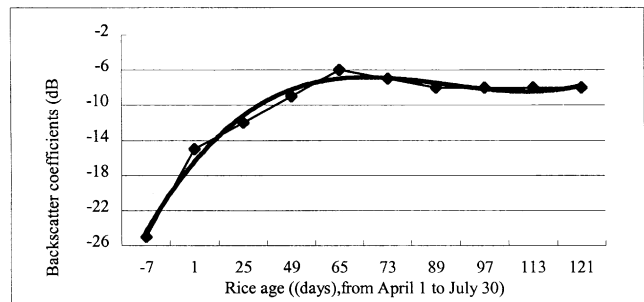


Fig. 1. Experimental backscatter model of rice.

we accumulated in our research efforts in the Zhaoqing test site since 1993 (Shao, Fan, et al., 1997; Shao et al., 1994; Shao et al., 1995a, 1995b), and is suitable for rice monitoring using Fine and Standard modes RADARSAT data (i.e., C–HH at 40–50° incidence angle). The backscatter coefficient from flooded rice fields before or just after transplanting is the same as for the water surfaces recorded by RADARSAT, around –25 dB. After transplanting, in the first 20 days, the backscatter coefficient from paddy rice increases to about –15 dB. Then, the rice enters the seedling-development period, from 20 to 45 days, and the backscatter coefficients from paddy rice fields increase to –12 dB. From 45 to 75 days, within the ear differentiation period, the backscatter coefficients from paddy rice fields increase further to –9 dB. In the middle of the ear differentiation period, at about 65 days, the backscatter coefficient reaches the highest point of –6 dB. Then, it gradually drops to –8 dB and maintains this value during the maturing period. This model can be used to predict the backscatter behavior of rice during its life cycle and relates changes in backscatter intensity to the rice age in days. Although different varieties and life spans of rice generate different backscatter behaviour, the form of the relationship is the same, allowing this model to be applied to other types of rice.

The empirical backscatter model is expressed as:

$$y = 0.0888x^3 - 1.9231x^2 + 13.155x - 35.767$$

## 5.2. Image processing

The multitemporal RADARSAT data processing for this study can be divided into four parts: geometric correction and co-registration, speckle noise reduction, classification, and postclassification processing. This was accomplished using the commercial PCI remote sensing image processing software. The methodology employed during this study was as follows.

(1) Register recently acquired image data to existing image data and topographic maps using ground control points and a digital elevation model (DEM). In order to simplify the classification and improve the classification efficiency, the forested mountainous areas were masked out and assigned to the forest class before classification, using the DEM. This was done automatically for a given elevation in the flood plain, with areas of elevation above 50 m assigned to the forest class, and the rest of the image area then classified using the methodology described below.

(2) An Enhanced Lee filter with a 5 × 5 window was used for speckle-filtering the radar imagery to remove the fading noise and small patches of cover before the classification.

(3) Using the ground truth data to identify the land-cover type, such as paddy rice, bananas, sugarcane, etc., and for the rice, class identify types with different life spans, such as medium mature rice. Delineate these targets as training areas and then classify the multitemporal radar images by apply-

ing a neural net classifier, which is available in the PCI software package. The training areas should be defined as precisely as possible in order to obtain an accurate classification output.

(4) Assign chosen colors to each of the classes, for example, assign the orange color to medium mature rice. A postclassification Sieve filter with a 7 × 7 window was then used to remove additional small patches. The land cover maps, crop maps, and rice maps were then produced following cartographic principles.

(5) Assess the classification accuracy with tools provided by PCI software and field identification from ground truth data. For the classification procedure, the total number of ground-truth verified land-cover types was 368 fields. A training sample of six fields per class was used to develop the classification procedure, while 12 fields per class were used for accuracy assessment.

(6) Calculate the area of each class. This allows the calculation of the acreage of rice production for each of the rice types using the empirical yield model. The empirical model for determining production based on rice life spans was provided by agronomists from Zhaoqing Branch, Academy of Agriculture of Guangdong Province, where this relationship between life span and yield/quality of rice was established through research efforts. The values used for this yield estimate were presented in Section 2.3.

Note the first two steps are used to produce the multitemporal RADARSAT image map. The last four steps are for producing the thematic maps derived from the RADARSAT data and the rice crop area and productivity estimate.

## 6. Results and discussion

### 6.1. Temporal backscatter behavior of rice

The ground measurement data clearly shows that several parameters remained unchanged as the rice crop grew (i.e., row spacing), while others showed significant temporal changes. Only plant water content, the height of the rice stem, and the leaf length have been selected for discussion in this paper, since they demonstrated distinct changes over a rice growth cycle, and provide a significant contribution to backscatter values. Fig. 2 shows the changes of rice height and leaf length measured from the spring to the summer of 1997. Measurements were taken for the height of the rice stem and the length of leaves 1, 2, 3, 4, and 5. Starting from the transplanting period, the height of the rice stem increased from 20 to about 100 cm, and reached its peak growth during the heading period. It remains at the same height for a period, then drops by about 5 cm, before stabilizing again at the lower height. The most obvious changes in rice over a given life cycle relate to the height of the stem. When rice matures, the weight of the head brings the height of the stem slightly lower. The variations of the measured five leaves were quite significant. Leaves 1 and 2

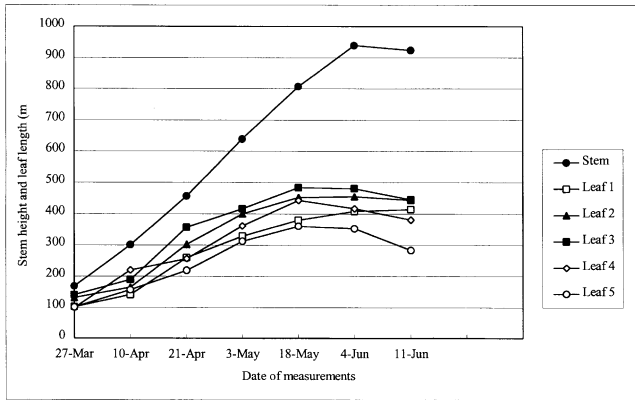


Fig. 2. Measurements of rice stem height and leaf length in 1997.

increase consistently and gradually with the growth of the rice plant. Leaves 3, 4, and 5 increased gradually as the rice grow, and reached a maximum at the ear differentiation stage in the middle of May. The measurements were only taken for medium mature rice. The structural parameters and plant water content are rice species-dependent. Different rice types growing in different geographic regions with varying ecological conditions results in rice having different structural parameters and water contents.

Fig. 3 shows the water content ( $C_w$ ) of rice measured from the spring to the summer of 1997. The water content is determined by measuring the weight of a cluster of fresh rice just after it has been cut ( $C_f$ ), drying the rice, and then re-measuring the weight of dry rice again ( $C_d$ ). The water content is calculated as  $C_w = (C_f - C_d) / C_f \times 100$  and presented as a percentage. For each measurement, there were 20 clusters of rice samples. As seen in Fig. 3, the rice has a high water content in its seedling-development period (80%) and during the ear differentiation period (85%). At the end of the ear differentiation period, the water content decreases slowly, and reaches its lowest point during the maturing

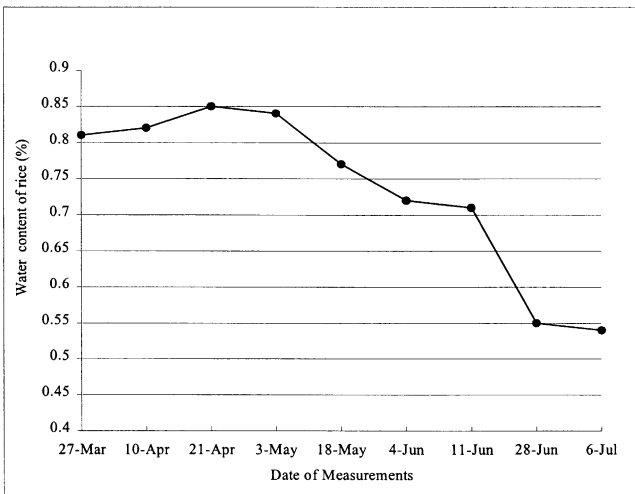


Fig. 3. Water content measurements of rice in 1997.

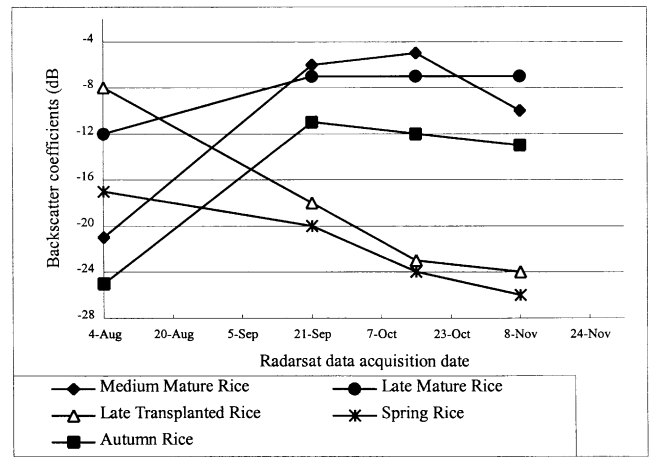


Fig. 4. Backscatter coefficients of rice as a function of time (1996). The calibration accuracy is approximately 1 dB.

period (55%). The water content of rice at its early stage is about 30% higher than during the maturing period.

Figs. 4 and 5 show the backscatter coefficients of rice extracted from the calibrated RADARSAT images acquired from the summer to the autumn of 1996 and from the spring to the summer of 1997, respectively. In Fig. 4, there are five types of rice: medium mature rice, late mature rice, late transplanted rice, spring rice, and autumn rice. The backscatter coefficient of late mature rice is 9 dB higher than medium mature rice on August 4. This is because the medium mature rice is still in the transplanting growth stage, having just been transplanted from the seedbed to the paddy field less than a week before. The seedling is thus very small, only 20 cm high, in the recovering stage, and therefore not as fresh and wet as the already recovered rice seedlings in the late mature rice paddies. Consequently, the backscatter coefficient is only 3 dB higher than the value for a still water surface. On November 8, the medium mature rice is in the late maturing period and nearly ready for harvest, but the late mature rice has just entered the

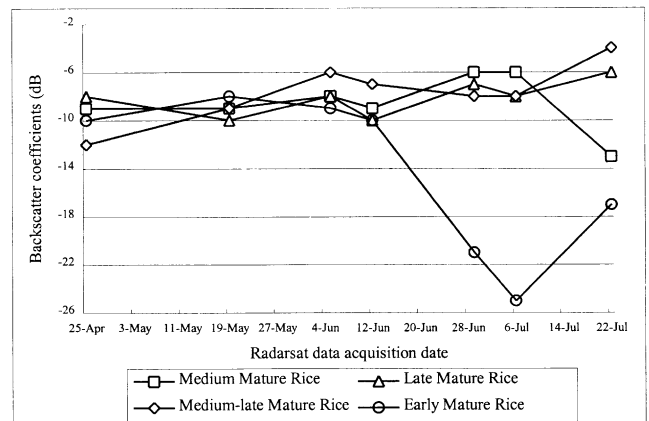


Fig. 5. Backscatter coefficients of rice as a function of time (1997). The calibration accuracy is approximately 1 dB.

maturing period and is wetter than the medium mature rice. In this case, the backscattering coefficient of the late mature rice is 3 dB higher than the value for medium mature rice. The late transplanted rice was transplanted about 25 days later than the normal spring rice, due to a cold spring and low temperatures in 1996. All 13 scenes of RADARSAT images acquired in 1996 were analyzed during this study, but only five scenes of the Fine mode images were used to produce Fig. 4. The RADARSAT image acquired on April 25, 1996 shows the backscatter coefficients of these fields to be very low, similar to a still water body. The backscatter coefficients from the RADARSAT images taken after April 25 increase gradually, until September (data not shown in Fig. 4) when the rice was harvested. The life span of this rice is relatively short, and the backscatter coefficients are lower.

In Fig. 5, there were four major types of rice with different growth cycles. With the knowledge gained from the rice backscatter behavior of 1996, we can distinguish between the rice types shown in Fig. 5. They are early mature rice, medium mature rice, medium–late mature rice, and late mature rice. Their life span is about 80, 100–115, 110–120, and 120–125 days, respectively. If a type of rice has a higher backscatter value in April, at the early stage or the seedling-development period, as found with late mature rice, then it was transplanted earlier than the other types of rice. If a type of rice has a higher backscatter coefficient in late July, during the maturing stage or the harvest period, the rice is harvested later than other types of rice, as found with medium–late mature rice and late mature rice. From Fig. 5, we can conclude that late mature rice has the longest life span. The medium–late mature rice was transplanted a few days later than medium mature rice and late mature rice, and harvested only slightly later than the medium mature rice. The medium mature rice was harvested before July 22. From Fig. 5, we can see that early mature rice was harvested before June 28. After that, it has very low backscatter coefficients since the paddy fields were re-flooded. It is concluded that between the early stage, 25 days after transplanting, and the late stage, 80 days after transplanting, we can distinguish rice with different life spans, which is important information for rice production estimation, because the life span is directly related to the yield and quality of rice. The farmer used to grow three rice crops a year in past, whereas now they only grow two rice crops a year and make more money from rice farming than in the past. This is largely attributed to the higher yields and better quality achieved with two long-growing varieties than three short-growth varieties.

The examples presented for spring rice and autumn rice types (Fig. 5) also demonstrate how farming activities can change within a year, switching between fishponds and rice fields. The spring rice was a rice field in the spring and then switched to a fishpond in the autumn. Conversely, the autumn rice was a fishpond in the spring then switched to

a rice field in the autumn. This farming practice is common in Zhaoqing area, as well as in many other parts of China. In general, this land-use change between fishponds and rice paddies implies that the quality of the field is less than excellent, and therefore the rice production is normally lower. The later three types of rice grow in cultivated lands of poor quality. The yield from this kind of land is generally lower than that from other areas. Based on the classification results of the 1996 multitemporal fine mode RADARSAT data set, a land cover map (Fig. 6) was produced showing five types of rice, as well as other vegetation and land-cover types.

The empirical backscatter model presented in Fig. 1 represents the backscatter behavior of medium–late mature rice. Medium–late mature rice is transplanted on April 1 and harvested on July 30. The late mature rice and medium mature rice are transplanted earlier than medium–late mature rice. Medium mature rice is harvested earlier than medium–late mature rice. This model can be applied to other types of rice and modified in accordance with the rice life span, transplant date, and harvest date. We can therefore use this model to calculate the backscatter coefficient of rice at a particular growth stage. During the maturing period for spring rice, it is also the wet season in both the Zhaoqing region and in southern China (Guo, Shao, Liao, Wang, & Liu ed., 1999a; Guo, Shao, & Wang ed., 1999b), so the backscatter coefficients of rice can be much higher than normal due to free canopy moisture from dew and rain effects. We must take this effect into account when we examine the backscatter behavior of targets, especially for vegetation.

These results imply that there are two important radar data acquisition time periods for rice monitoring: at the end of the transplanting and seedling recovery period, and at the beginning of the ear differentiation period. In the study area, the transplanting and seedling recovery stage is middle–late April for spring rice and middle–late August for autumn rice. Mid-May is the ear differentiation period for spring rice, while mid-September is the time for autumn rice. Thus, for determining the acreage of planted rice, two radar data acquisitions are required: one in middle–late April during the seedling developing period, and another in the middle of May during the ear differentiation period. The use of change detection techniques between the first and second data acquisitions allows the difference between rice and other land-cover types to be determined. These two data sets can be used for the automatic classification because the difference in backscatter between paddy fields versus other land-cover types on these two dates is much larger for rice than any other land-cover types. Therefore, after the second radar data acquisition, we can map the area of rice cultivation. For rice production estimation, at least three radar data acquisitions are required: one in mid–late April, one in the middle of May, and one at the end of June. For autumn rice or late season rice, the corresponding date can be

## Land Cover Map of Dinghu Site Based on Multi-temporal RADARSAT Images (1996)

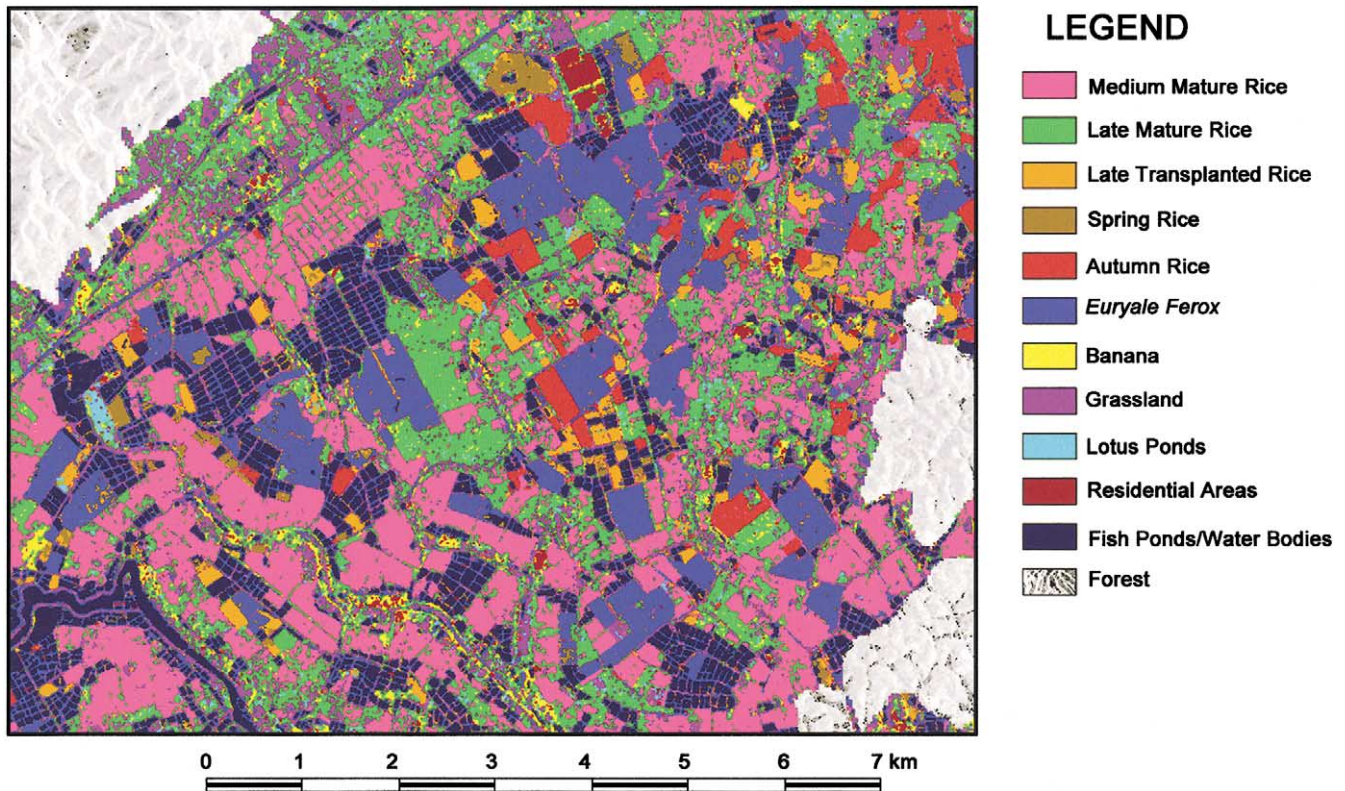


Fig. 6. Land cover map of Dinghu site, China based on multitemporal RADARSAT images for 1996. See text for details.

found by checking the rice growth calendar. The last data acquisition provides information about the growth status of rice, whether it is healthy or not, or if it has been harvested due to early maturity or for other reasons, such as poor soil conditions or diseases.

### 6.2. Image output products

A land cover map (Fig. 6) was produced based on the land cover classification of five scenes of Fine mode RADARSAT images acquired in 1996. Five types of rice, four types of vegetation, and other targets were classified and are shown on the land cover map. A false-color composite was produced using the multitemporal Standard mode RADARSAT images acquired in the spring of 1997 by combining the image acquired on July 22 (in red), the mean intensity of images acquired on April 25 and May 19 (in green), and the mean intensity of images acquired on June 4, 12, and 28 (in blue). This image is presented in Fig. 7. Essentially, if a target is dominantly red, it has strong backscatter in July, if a target is dominantly green, it has strong backscatter in June, and if a target is dominantly blue, it has stronger backscatter in April and May. Therefore, the colors in Fig. 7 represent the intensity of backscatter

coefficient for various targets, for example, the cyan color, orange color, magenta color, and green color represent the medium mature rice, late mature rice, medium–late mature rice, and early mature rice, respectively.

Further, detailed backscatter behavior of rice can be inferred from the results presented in Fig. 5. If a type of rice has a higher backscatter value in April, at the early stage or seedling development period, as found with late mature rice, then it was transplanted earlier than the other types of rice. If a type of rice has a higher backscatter coefficient in July, during the maturity stage or the harvest period, the rice was harvested later than the other types of rice, as found with late mature rice, and medium–late mature rice. From Fig. 5, we can conclude that late mature rice has the longest lifetime with higher backscatter coefficients in all three bands, represented as a bright orange color. The medium–late mature rice was transplanted a few days later than the late mature rice, and harvested later as well. It has a lower backscatter in blue, and shows up as magenta in the multitemporal RADARSAT image. The medium mature rice was harvested before July 22, and displayed as a cyan color on Fig. 7. From Fig. 5, we can see that early mature rice is harvested before June 28. It has very low backscatter coefficients during the early harvest period, and thus shows up as a bright green color on Fig. 7.

## Multi-temporal RADARSAT Image Zhaoqing Test Site (1997)

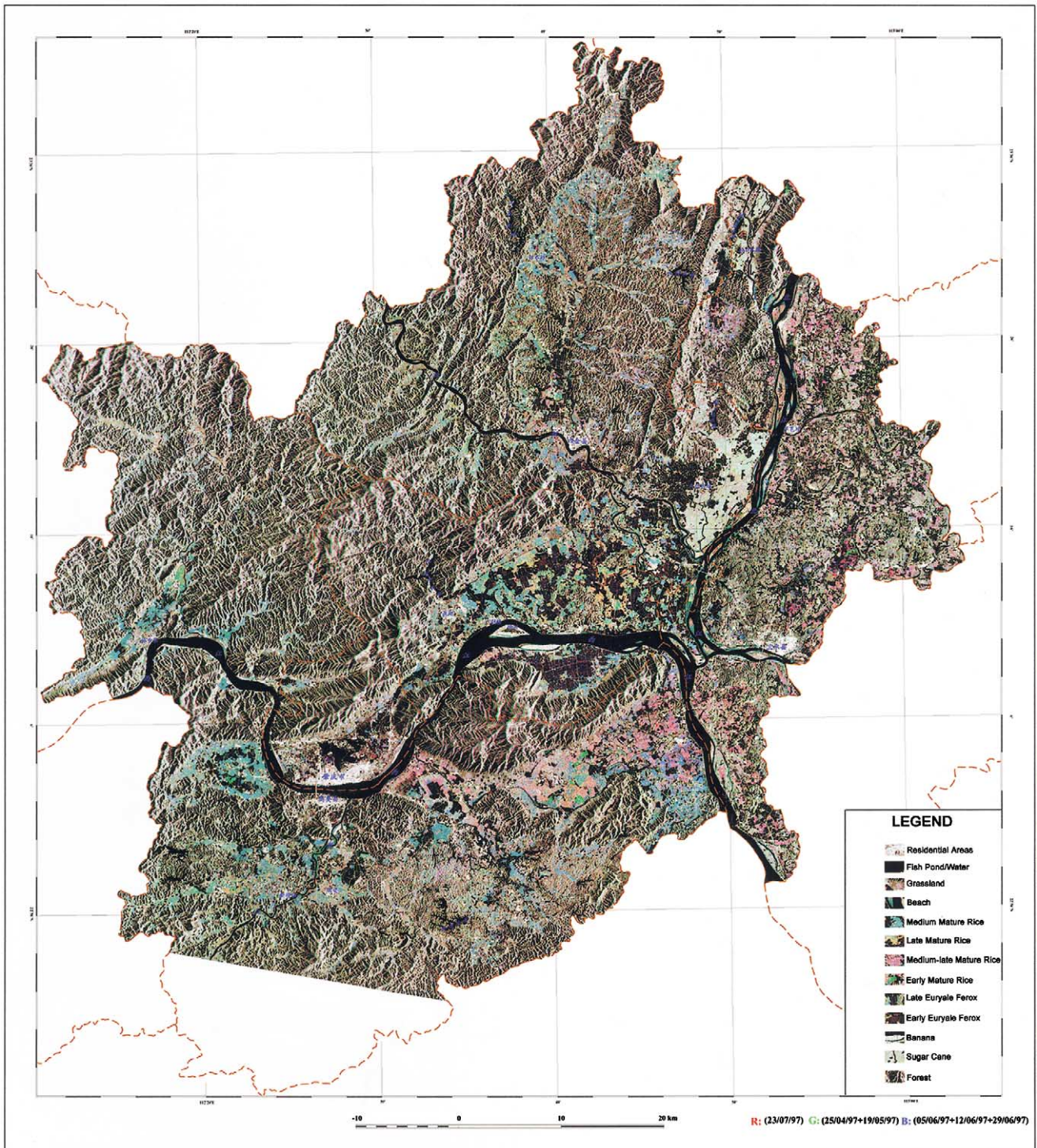


Fig. 7. Multitemporal RADARSAT image of Zhaoqing test site, China for 1997. See text for details.

### 6.3. Classification results

The classification accuracy was automatically calculated by the PCI software based on the training and testing fields identified in Section 5.2, step 5 above. Table 3 shows the

confusion matrix for the classification using the neural net classifier. The average accuracy of the classification is 90.10% and the overall accuracy is 91.49%. The  $\kappa$  coefficient equals 0.89699 with a standard deviation of 0.00135, which equals  $0.89699 \pm 0.00347$  at a confidence level of

Table 3  
The confuse matrix for the land cover classification using the neutral net classifier

|          | Class 1 | Class 2 | Class 3 | Class 4 | Class 5 | Class 6 | Class 7 | Class 8 | Class 9 | Class 10 | Class 11 | Class 12 | Class 13 |
|----------|---------|---------|---------|---------|---------|---------|---------|---------|---------|----------|----------|----------|----------|
| Class 1  | 94.2    | 5.7     | 0.0     | 0.0     | 0.0     | 0.0     | 0.0     | 0.0     | 0.0     | 0.0      | 0.0      | 0.0      | 0.1      |
| Class 2  | 0.1     | 99.8    | 0.0     | 0.0     | 0.0     | 0.1     | 0.0     | 0.0     | 0.0     | 0.0      | 0.0      | 0.0      | 0.0      |
| Class 3  | 0.0     | 0.0     | 86.6    | 0.6     | 0.1     | 4.4     | 0.0     | 1.2     | 4.5     | 0.0      | 0.0      | 0.0      | 2.6      |
| Class 4  | 0.0     | 0.0     | 0.0     | 98.0    | 0.8     | 0.9     | 0.0     | 0.3     | 0.0     | 0.0      | 0.0      | 0.0      | 0.0      |
| Class 5  | 0.0     | 0.1     | 0.0     | 3.9     | 94.2    | 1.8     | 0.0     | 0.1     | 0.0     | 0.0      | 0.0      | 0.0      | 0.0      |
| Class 6  | 0.0     | 1.1     | 0.0     | 1.1     | 0.5     | 97.2    | 0.0     | 0.0     | 0.0     | 0.0      | 0.0      | 0.0      | 0.1      |
| Class 7  | 0.0     | 0.0     | 0.0     | 0.5     | 0.3     | 0.0     | 84.0    | 12.8    | 0.0     | 2.5      | 0.0      | 0.0      | 0.0      |
| Class 8  | 0.0     | 0.0     | 0.2     | 1.1     | 0.1     | 0.1     | 8.1     | 90.1    | 0.2     | 0.2      | 0.0      | 0.0      | 0.0      |
| Class 9  | 0.0     | 0.0     | 0.6     | 0.2     | 0.0     | 0.6     | 0.0     | 0.0     | 96.4    | 0.0      | 0.0      | 0.0      | 2.1      |
| Class 10 | 0.0     | 0.0     | 0.2     | 0.6     | 0.5     | 0.4     | 15.8    | 6.3     | 0.0     | 76.2     | 0.0      | 0.0      | 0.0      |
| Class 11 | 1.3     | 0.0     | 0.0     | 0.0     | 0.0     | 0.0     | 0.0     | 0.0     | 0.0     | 0.0      | 98.7     | 0.0      | 0.0      |
| Class 12 | 0.0     | 0.0     | 0.0     | 0.0     | 0.0     | 0.0     | 0.0     | 0.0     | 0.0     | 0.0      | 0.0      | 100.0    | 0.0      |
| Class 13 | 1.8     | 0.0     | 32.3    | 0.0     | 0.0     | 0.7     | 0.0     | 0.0     | 9.2     | 0.0      | 0.1      | 0.0      | 55.9     |

Class 1: early *Euryale forex*; Class 2: late *Euryale forex*; Class 3: medium mature rice; Class 4: late mature rice; Class 5: medium–late mature rice; Class 6: grass; Class 7: banana; Class 8: sugar cane; Class 9: early mature rice; Class 10: residential areas; Class 11: fish ponds/water; Class 12: forest; Class 13: Beach.

99%,  $\pm 0.00264$  at a confidence level of 95%, and  $\pm 0.00221$  at a confidence level of 90%. The classification accuracy was verified as described in Section 5.2. After the postclassification filtering and enhancement, the overall accuracy of the land cover classification was 97%.

Four types of rice, as well as four types of vegetation and other targets, were classified, as shown on the land cover classification (Fig. 6) and the RADARSAT image map (Fig. 7). Based on the classification of the seven RADARSAT images, a rice distribution map was produced by combining classes, so as to display only the different rice crops, water bodies, forested land, residential areas, and nonrice targets (Fig. 8).

According to the meteorological data, 1997 was a good year for agriculture. For this reason, the yield should be at the “normal” level. We can thus use the “typical” yields of rice with different life spans to calculate the rice production of the imaged area. Table 4 shows the statistical results of calculating this rice area for rice varieties and other targets for Shihui County, Gaoyao County, Shanshui County and Dinghu administration region, and Duanzhou administration region, covering a total area of 4998.1 km<sup>2</sup> (as shown in Fig. 7). The total production of this area is 404,227 mu  $\times$  0.45 tons = 181,902.15 tons for medium mature rice, 379,179 mu  $\times$  0.55 ton = 208,548.45 tons for late mature rice, 349,272 mu  $\times$  0.5 ton = 174,636.0 tons for medium–late mature rice, and 51,366 mu  $\times$  0.35 ton = 17,978.1 tons for early mature rice. The total rice production for these three counties and two administration regions is thus 583,064.7 tons. This rice yield estimate, in units of mu for the different rice types, was obtained from empirical meteorological-based models provided by the agronomists from the Academy of Agriculture of Guangdong Province, described previously.

The accuracy of the rice production estimate is difficult to assess because it is only an approximate estimate based on an empirical model, and there is no reliable “ground-truth” data with which to compare the results. SAR data can be used to infer the life span of the rice from the empirical

model presented in Fig. 1. The rice yield should be determined by a meteorological model and farming practices. In this case, the environmental conditions were “normal” and the standard yield model could be used. In other years, a different yield model may be required as a consequence of those years’ environmental conditions. The quality of these products created from multitemporal RADARSAT data demonstrates the feasibility and effectiveness of RADARSAT data for rice crop monitoring. In general, the end-user agencies and local authorities were very happy with the results, and are implementing the methodology operationally due to the success of this pilot project.

## 7. Scenario for operational rice monitoring and production estimation

Researchers in the Institute of Remote Sensing Applications (IRSA), through a program entitled “SAR Technology for Rice Growth Status Monitoring and Land Cover Mapping,” supported by the National High Technology Program, have worked to provide information on rice growth status and production, to both national and local governmental agencies. This information is provided to commercial users as well. The final goal of this project is to establish an operational rice monitoring and production estimation system for China. This paper presented the research achievements of this program in the above sections. Fig. 9 illustrates a pilot scenario for operational rice monitoring and yield estimation, and outlines the operating procedures developed during this research. The procedure can be divided into six parts, described below.

### 7.1. Data input: multitemporal and multiparameter radar data

The radar data provides up-to-date information on current rice growth conditions and an accurate estimate of the

## Rice Distribution Map of Zhaoqing Test Site (1997)

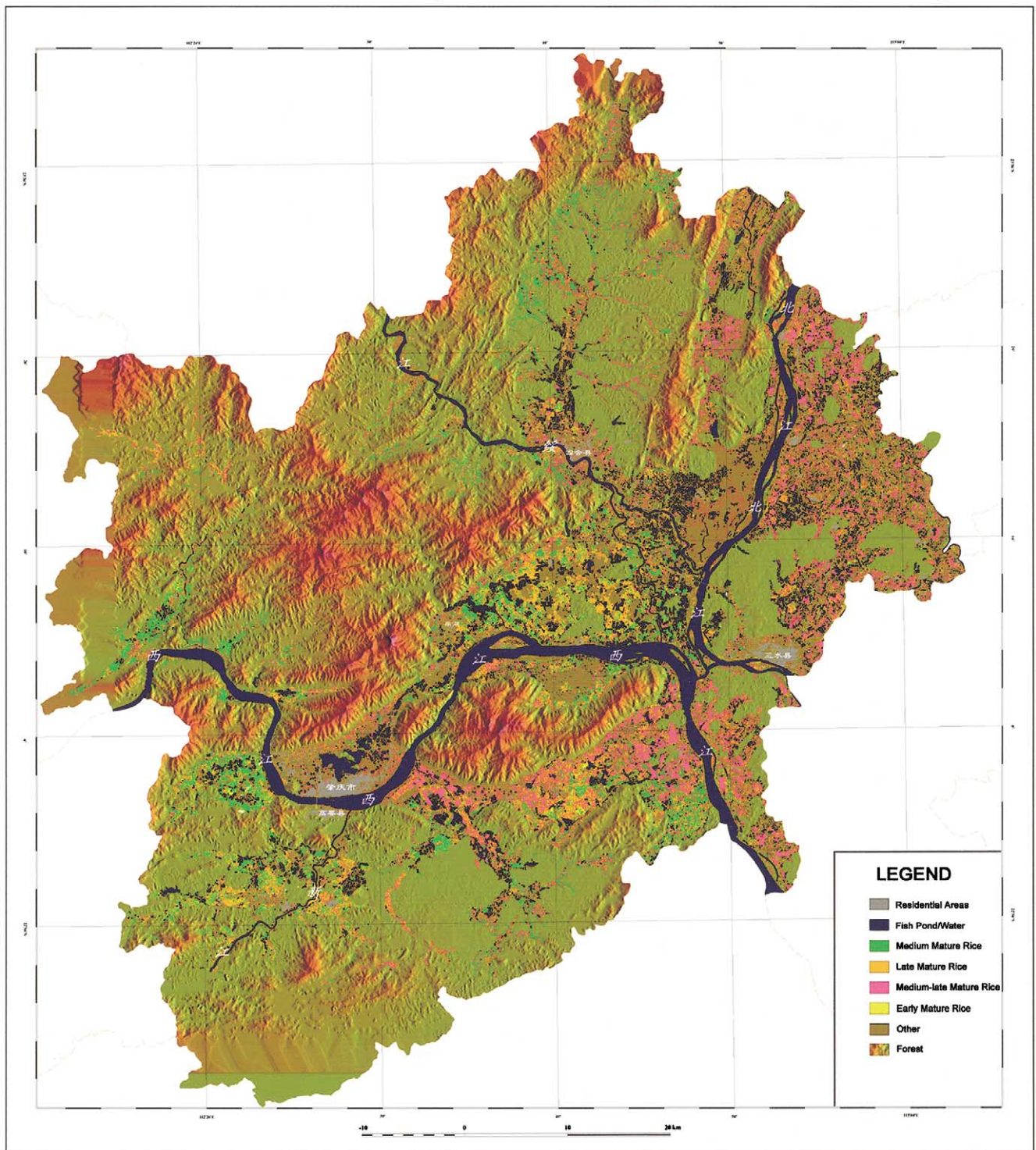


Fig. 8. Rice distribution map of Zhaoqing test site, China for 1997.

area of rice production. For single-channel radar data, like RADARSAT, at least three data acquisitions are required. In general, these are one about 20 days after the transplanting stage (data source A), one at the end of seedling-develop-

ment period about 50 days after the transplanting stage (data source B), and another data acquisition just prior to harvest (data source C). For multichannel radar data (i.e., multi-frequency and/or multipolarization), one data acquisition is

Table 4  
Statistical results of land cover classes in Zhaoqing

| Class                   | Hectarage (m <sup>2</sup> ) | Percent (%) |
|-------------------------|-----------------------------|-------------|
| <i>Euryale ferox</i> 1  | 87,012,656.0                | 1.74        |
| <i>Euryale ferox</i> 2  | 54,568,124.0                | 1.09        |
| Medium mature rice      | 269,454,368.0               | 1.09        |
| Late mature rice        | 252,760,230.0               | 5.39        |
| Medium–late mature rice | 232,824,528.0               | 4.66        |
| Early mature rice       | 34,240,312.0                | 0.69        |
| Grassland               | 430,799,520.0               | 8.62        |
| Banana field            | 35,338,124.0                | 0.71        |
| Sugar cane field        | 43,732,656.0                | 0.87        |
| Residence areas         | 59,249,844.0                | 1.19        |
| Water body              | 320,362,016.0               | 6.41        |
| Forest                  | 3,166,174,976.0             | 63.34       |
| Beach land              | 11,598,906.0                | 0.23        |

required during the early stage of rice growth and another radar data acquisition at the end of the heading period or the beginning of the maturing period, just prior to harvest.

7.2. Static supporting data

A DEM is required to understand the rice distribution limitations and to aid in image processing. In addition, soil maps help to know the soil quality and its effect on rice yield. Knowledge of the crop calendar is needed to decide the optimum date for radar data acquisition, and explain the rice growth stages at the image acquisition time. The crop calendar may shift a few days at the transplanting period, in accordance with local environmental conditions.

7.3. Dynamic supporting data

Meteorological data, including temperature, total solar illumination, rainfall, etc., are critical elements needed to determine the yield of rice on a regional scale. The current rice yield models are based on meteorological data, and will be used synergistically with the information extracted from the SAR data. Knowledge of tillage activities provides information on the seeding of the rice and transplanting methods, which is directly related to the yield. In the early stages of the program, data sources A and B (see Section 7.1) will be used to determine the rice area. Data source C will then be used for determining the yield or productivity estimate.

7.4. Supporting database

There are a series of database and numerical models needed to support the image processing and the yield estimation work. These are the following.

(A) Rice yield model based on the input source of static and dynamic data, which directly go into the rice yield estimation procedure.

(B) Database ground control points (GCPS) are collected and used to register the acquired imagery to the stored DEM, as well as to other images or data from different dates or sources.

(C) Representative training areas for classification are selected for both rice and other targets. In general, the sites chosen should be regular and stable.

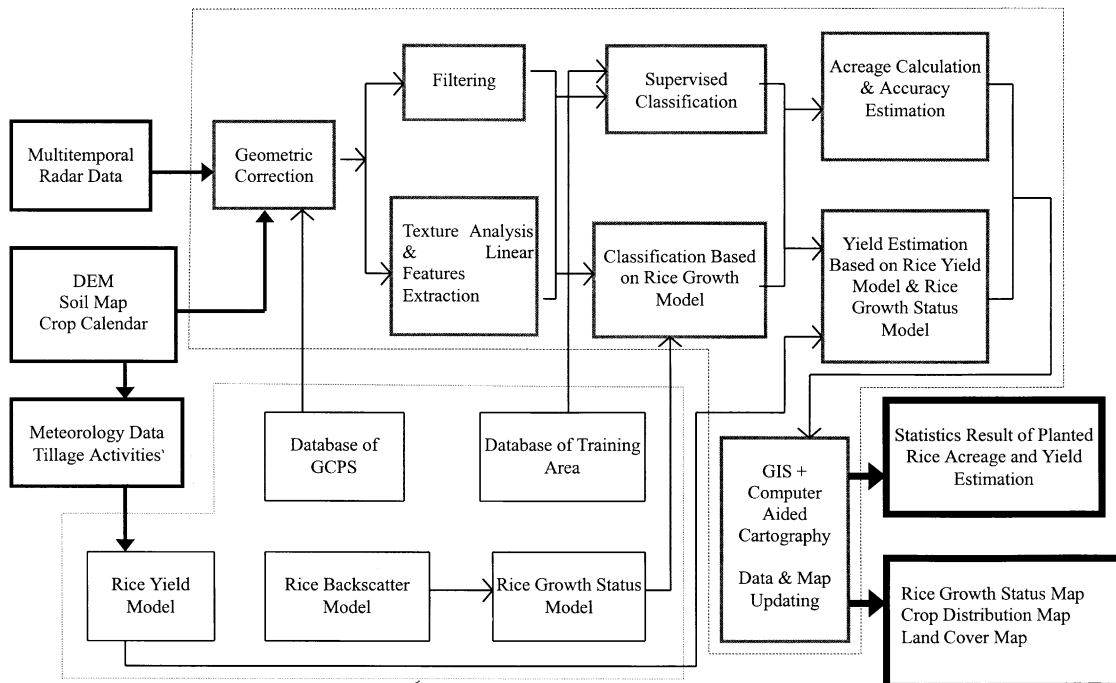


Fig. 9. An outline for operational rice growth monitoring and yield estimation using SAR data.

(D) A rice theoretical backscatter model is a numerical model based on radiative transfer theory, which can be used to help explain rice backscatter behavior. An empirical rice backscatter model (Fig. 1) was established by studying the multitemporal RADARSAT data of 1996 and 1997. These two models can be used to classify the radar data and/or correct and modify the classification results.

### 7.5. Image processing

The following summarizes the image processing methodology.

(A) Registration of the imagery to existing data and maps using a DEM and GCPs.

(B) Filtering to remove the speckle noise and small patches before and after classification.

(C) Extraction of linear features such as ditches between fields. The width of these linear features is enlarged by the corner reflection effect, allowing the linear features to be easily seen on an image. The actual area of these linear features should be calculated and considered when calculating the area of rice. An algorithm for linear feature extraction and how to estimate the actual area of these linear features should be developed for rice area estimations and is a topic in need of further research.

(D) Classification to separate different types of rice and determine the classification accuracy of rice and other targets. In this study, a neural network classifier from the PCI software package was used to classify the multitemporal RADARSAT data.

(E) Based on the classification and linear feature extraction, a precise calculation of the area of rice can be made. Combined with the rice yield model and the rice experimental backscatter model, we can make the first yield estimation and forecast the area and production of rice. Meteorological data can help in the estimation and forecasting of the yield. During the harvest season, there may be some hazardous weather such as summer storms and flooding. Under these conditions, we will need a third data acquisition to determine if the rice is in a healthy condition.

(F) Create new maps, and update existing databases with the new results and information.

### 7.6. Output

The following output products will be produced by the rice monitoring and yield estimation system.

(A) Statistical results on rice crop area and potential production: According to the county and provincial administration boundaries, we can provide statistical results on rice area and potential production at a county level, or a regional level as shown in Table 4.

(B) Maps: In 1997, the output of this project included four map products (Guo et al., 1999a,b): (1) the multitemporal RADARSAT image map of Zhaoqing test site (Fig. 7); (2) the land cover map (not shown but similar to Fig. 6);

(3) the crop distribution map; and (4) the rice distribution map (Fig. 8). In 1999, the output of this project included two map products (Guo et al., 1999a,b): (1) the multitemporal RADARSAT image map of the Pearl River Delta test site and (2) the rice distribution map. Table 1 shows the acquisition dates of the RADARSAT images with a total coverage of 40,000 km<sup>2</sup> in 1999.

## 8. Discussion and conclusions

The results presented in this paper have provided confidence that multitemporal RADARSAT data is capable of rice mapping and can provide input to production estimation. However, the results are far from perfect, and additional work remains to be done. Figs. 2 and 3 show two critical factors that determine the backscatter coefficients of rice, which are the moisture of the rice canopy and the stem height and leaf length of rice. In fact, as rice grows, the plant moisture is decreasing; however, the stem height and leaf length is increasing. The C–HH RADARSAT only measures one channel at a time, which is the backscatter coefficient of rice at C–HH and a fixed incidence angle. From one measurement, it is hard to estimate more than one parameter of a target. It is obvious that we need multifrequency and multipolarization data to resolve this problem. The multifrequency and multipolarization SAR imagery does show a better capability for discriminating targets. Fig. 10 can be used as an example to illustrate this point.

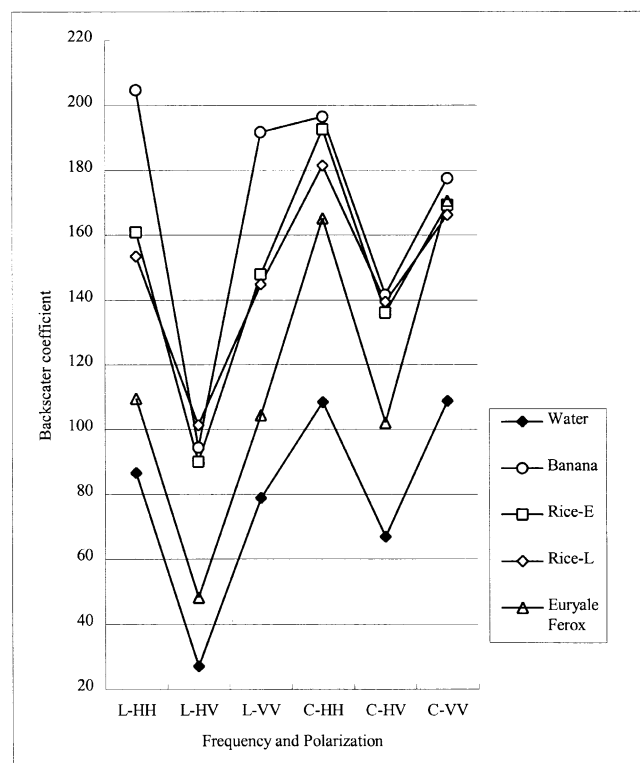


Fig. 10. Backscatter coefficients from SIR-C data as a function of frequency and polarization.

Fig. 10 shows the backscatter coefficients (in DN format) of targets as a function of frequency and polarization. It is produced by averaging the DN for pixels taken from a square area of 20 pixels by 20 lines of the absolutely calibrated SIR-C/X-SAR imagery for both C- and L-bands, HH, HV, and VV polarizations. On April 18, the early transplanted rice (Rice-E) and the late transplanted rice (Rice-L) were just transplanted, starting the seedling development period. The height of the rice seedlings of both rice types was about 20–30 cm. The early transplanted rice was 1 week older than the late transplanted rice, and the backscatter coefficients were slightly higher, as shown in Fig. 10. Even though the rice has only very small single seedlings standing in open water, the longer L-band wavelength can show the difference between rice and water (Shao, Liu, et al., 1997). It is noted from Fig. 10 that at shorter wavelengths, rice has a much stronger response. Its response to HH polarization is higher than VV polarization. Its response to HV polarization is much lower, which indicates rice seedlings produce a double bounce effect between the water surface and the rice stem. Banana trees have very similar backscatter behavior except they have a much stronger return due to their large, upward growing leaves. In contrast to vertical structured vegetation, such as rice and banana, the *Euryale ferox* (a water plant in the same family as lotus), with large flat leaves laying on the surface of the water, has higher backscatter at VV polarization than HH polarization. The flat leaves act as a slightly rough surface. Generally speaking, slightly rough surfaces have stronger reflections at VV polarization than HH polarization, which is clearly shown in Fig. 10.

Fig. 10 shows better rice discriminating capability is possible with multifrequency and multipolarization SAR data. It is anticipated that the utilization of multifrequency and multipolarization SAR imagery will provide more information for separating all land cover targets and reduce the data acquisition requirements. Fig. 10 illustrates that one data acquisition of multifrequency and multipolarization SAR imagery can discriminate two types of rice and other targets as well. Therefore, we can reduce the data acquisition from two dates at the early rice growth stages to only one. We suggested above that rice production estimates using multitemporal, single-channel SAR images requires three radar data acquisitions taken at three stages of crop growth: at the end of the seedling-development period, in the ear differentiation period, and at the beginning of the harvest period. Alternatively, if multichannel SAR imagery (both frequency and polarization) is available, data acquisition requirements may reduce to only two: at the end of the seedling period and at the beginning of the harvest period.

## Acknowledgments

The 863 National High Technology Program sponsored by the Ministry of Science and Technology funds this research work. The authors wish to take this opportunity to

express their sincere acknowledgment to the members of the 863-308 Expert Group: Prof. H.D. Guo, J.M. Xu, Z.M. Yang, Z.Q. Wei, X.G. Ling, X.T. Zhou, G.Q. Ni, and Dr. Y.J. Wu of MST, Mr. J.L. Miao of the 863-308 office. Special appreciation goes to Dr. Fred Campbell of the Canada Center for Remote Sensing for his kind support to this research.

## References

- Anys, H., & He, D. C. (1995). Evaluation of textural and multipolarization radar features for crop classification. *IEEE Transactions on Geoscience and Remote Sensing*, 33 (5), 1170–1181.
- Brisco, B., & Brown, R. J. (1998). Agricultural applications with RADAR. In: F. Henderson, & A. Lewis (Eds.), *Manual of remote sensing principles and applications of imaging radar* (3rd ed). Washington, DC: American Society of Photogrammetry and Remote Sensing (Chap. 7).
- Campbell, F., Ryerson, R., & Brown, R. (1995). GlobeSAR: a Canadian radar remote sensing program. *GEOCARTO International*, 10 (3), 3–8.
- Chauhan, N. S., LeVine, D. M., & Lang, R. H. (1994). Discrete scatter model for microwave radar and radiometer response to cone: comparison of theory and data. *IEEE Transactions on Geoscience and Remote Sensing*, 32, 416–426.
- Dobson, M. C., Pierce, L., Sarabandi, K., Ulaby, F. T., & Sharik, T. (1992). Preliminary analysis of ERS-1 SAR for forest ecosystem studies. *IEEE Transactions on Geoscience and Remote Sensing*, 30, 203–211.
- El-Rayes, M. A., & Ulaby, F. T. (1987). Microwave dielectric spectrum of vegetation. Part I. Experimental observation. *IEEE Transactions on Geoscience and Remote Sensing*, 25, 541–549.
- Engheta, N., & Elachi, C. (1982). Radar scattering from a diffuse vegetation layer over a smooth surface. *IEEE Transactions on Geoscience and Remote Sensing*, GE 20 (2), 212–216.
- Freeman, A., Durden, S., & Zimmerman, R. (1992). Mapping subtropical vegetation using multifrequency multipolarization SAR data. In: Proceedings of IGARSS'92, Houston, TX. (pp. 1686–1689).
- Guo, H., & Shao, Y. (1997). Airborne dual-band, full polarimetric SAR information analysis. *Journal of Remote Sensing*, 1 (2), 94–100. Science Press, Beijing, China (in Chinese).
- Guo H., Shao Y., Liao J., Wang C., & Liu H. (Eds.). (1999a). Analysis of Radar Remote Sensing Imagery in China. Science Press, Beijing, China (in Chinese).
- Guo H., Shao Y., & Wang C., (Eds.). (1999b). Radar for Earth Observation: Theory and Applications. Science Press, Beijing, China (in Chinese).
- Guo, H., Wang, C., Liao, J., Shao, Y., & Wei, C. (1995). Dual-frequency and quad-polarization SAR observations in Zhaoqing region, China. *GEOCARTO International*, 10 (3), 79–86.
- Karam, M. A., & Fung, A. K. (1988). Electromagnetic scattering from a layer of finite length, randomly oriented, dielectric, circular cylinders over a rough interface with application to vegetation. *International Journal of Remote Sensing*, 9 (6), 1109–1134.
- Kasischke, E. S., & Christensen Jr., N. L. (1990). Connecting forest ecosystem and microwave backscatter models. *International Journal of Remote Sensing*, 11, 1277–1298.
- Kurosu, T., Fujita, M., & Chiba, K. (1995). Monitoring of rice crop growth from space using the ERS-1 C-band SAR. *IEEE Transactions on Geoscience and Remote Sensing*, 33 (4), 1092–1096.
- Kurosu, T., Fujita, M., & Chiba, K. (1997). The identification of rice fields using multi-temporal ERS-1 C-band SAR data. *International Journal of Remote Sensing*, 18 (14), 2953–2965.
- Le Toan, T., Laur, H., Mougin, E., & Lopes, A. (1989). Multitemporal and dual-polarization observations of agricultural vegetation covers by X-band SAR images. *IEEE Transactions on Geoscience and Remote Sensing*, 27, 709–717.
- Le Toan, T., Ribbes, F., Floury, N., Wang, L., Kong, J., Kurosu, T., & Fujita, M. (1997). Rice crop mapping and monitoring using ERS-1 data based

- on experiment and modeling results. *IEEE Transactions on Geoscience and Remote Sensing*, 35 (1), 41–56.
- Liu, H., Shao, Y., & Wang, C. (1997). Multitemporal RADARSAT data for rice classification in Zhaoqing, Guangdong Province. *Land Resource Remote Sensing*, 4, 1–6 (in Chinese).
- Matzler, C. (1994). Microwave (1–100 GHz) dielectric model of leaves. *IEEE Transactions on Geoscience and Remote Sensing*, 32, 947–949.
- McDonald, R. B., & Hall, F. C. (1980). Global crop forecasting. *Science*, 208, 670–679.
- Schotten, C. G. J., van Rooy, W. W. L., & Janssen, L. L. F. (1995). Assessment of the capabilities of multitemporal ERS-1 SAR data to discriminate between agricultural crops. *International Journal of Remote Sensing*, 16, 2619–2637.
- Shao, Y., Fan, X., Wang, C., & Liu, H. (1997). Estimation rice growth stage using RADARSAT data. *Proceedings of Geoscience and Remote Sensing, IEEE*, 4 (Singapore).
- Shao, Y., Guo, H., Liu, H., Li, J., & Lu, X. (1995a). Effect of polarization of GlobeSAR data on vegetation discrimination. *GEOCARTO International*, 10 (3), 71–76.
- Shao, Y., & Guo, H. (1995b). The GlobeSAR Data for Vegetation Discrimination. In: H. Guo (Eds.), *Microwave Remote Sensing for Earth Observation*. Science Press, Beijing, China (pp. 195–201).
- Shao, Y., Guo, H., Liu, H., & Lu, X. (1996). GlobeSAR data for agriculture applications — potentials and limitations. In: *Proceedings of the second Asia regional GlobeSAR workshop* (pp. 79–83). Science Press.
- Shao, Y., Liu, H., Lu, X., & Guo, H. (1997). Effect of frequency and polarization on target detection. IEAS'97 and IWGIS'97, Beijing.
- Shao, Y., Verjee, F., & Staples, S. (1997). Cutting through cloud. In: GIS Asia Pacific, October/November, Singapore.
- Shao, Y., Wang, C., Fan, X., & Liu, H. (1997). Evaluation of SAR image for rice monitoring and land cover mapping. In: Presented at Geomatics in Era of RADARSAT, Ottawa, Canada.
- Soares, J. V., Bernard, R. D., & Vidal-Madjar, D. (1987). Spatial and temporal behavior of a large agricultural area as observed from airborne C-band scatterometer and thermal infrared radiometer. *International Journal of Remote Sensing*, 8 (7), 981–996.
- Soares, J. V., Renn, C. D., Formaggio, A. R., Yanasse, C. F., & Frery, A. C. (1997). An investigation of the selection of texture features for crop discrimination using SAR imagery. *Remote Sensing of Environment*, 59, 234–247.
- Stofan, E. R., Evans, D. L., Schmillius, C., et al (1995). Overview of results of spaceborne imaging radar-C, X-band synthetic aperture radar (SIR-C/X-SAR). *IEEE Transactions on Geoscience and Remote Sensing*, 33, 817–828.
- Ulaby, F. T., Li, R. Y., & Shanmugan, K. S. (1982). Crop classification using airborne radar and Landsat data. *IEEE Transactions on Geoscience and Remote Sensing, GE* 20 (1), 42–50.
- Ulaby, F. T., Moore, R. E., & Fung, A. K. (1981). *Microwave remote sensing: active and passive* vols. 1–3. Addison-Wesley Publishing.
- Ulaby, F. T., Sarabandi, K., McDonald, K. C., Whitt, M., & Dobson, M. C. (1990). Michigan microwave canopy scattering model (MIMICS). *International Journal of Remote Sensing*, 11, 1223–1253.
- Zhao, R., Wang, Y., & Dai, J. (Eds.). (1996). *Remote Sensing for Dynamic Rice Monitoring and Production Estimation*. Chinese Science and Technology Press, Beijing, China.
- Zebker, H. A., Van Zyl, J. J., et al (1991). Calibrated imaging radar polarimetry: techniques example and applications. *IEEE Transactions on Geoscience and Remote Sensing*, 29, 942–961.